QUANTITATIVE CHARACTERIZATION OF ADVECTIVE LOSSES IN A FALLING PARTICLE RECEIVER

GUILLERMO ANAYA[1], CLIFFORD HO[1], JESUS ORTEGA[2] & PETER VOROBIEFF[2]
[1]Sandia National Laboratories, USA
[2]University of New Mexico, USA

ABSTRACT
Concentrating solar power receivers use a thermal medium for energy storage. For falling particle receivers, ceramic particles are used both as the thermal storage and transfer medium. Inside the receiver described here, a gravity-driven particle curtain is irradiated through an open cavity with about 1 MW/m^2 of concentrated sunlight provided by a heliostat field. While this design offers important advantages, including high storage temperatures, there are some challenges associated with the design, such as advective particle loss from the receiver aperture. During operation plumes of particles being expelled out of the receiver cavity can be observed, resulting in heat/mass losses and an overall decrease in efficiency. We developed a non-intrusive measurement system to estimate these advective losses from the cavity of the receiver. It is based on an application of Particle Image Velocimetry (PIV) techniques to sets of thermograms obtained from a high-speed infrared camera. Both laboratory scale and field scale tests were conducted to validate the measurement process, after which we used field data to estimate efficiency losses, which proved to be modest.
Keywords: concentrating solar power, falling particle receivers, diagnostics.

1 INTRODUCTION

As the energy consumption demand keeps increasing around the world, so does the interest into implementation of renewable energy systems as an alternative to fossil fuels. Other driving factors behind the growth of interest to renewable energy are the environmental impacts and the limited accessible supply of fossil fuels. Moreover, fossil fuel availability may fluctuate due to a variety of reasons including politics and war. Here renewable energy systems have a distinct advantage of using local, replenishable, inexhaustible energy sources with a lower impact on the environment. The type of renewable energy systems discussed in this study is solar energy: approximately 173,000 terawatts of solar energy arrive at our planet continuously. Utilizing just a small percentage of that energy would suffice to meet the world energy demand [1].

Multiple types of systems are being developed with the intention of taking advantage of such an abundant resource, photovoltaic panels being the most popular one. Photovoltaic panels offer the convenience of transforming solar energy directly into electricity. However, most of the market available offer photovoltaic panels with an efficiency beginning at 6% to 20%. In photovoltaic panels most of solar energy is converted into waste heat, thus generating overheating problems that affect the efficiency of the system [2]. Another type of system used to take advantage of the energy provided by the sun are solar collectors that transform solar radiance into thermal energy. Some of these systems allow for thermal energy collection at temperatures above 600°C, which allows for higher operational efficiencies. Central receivers for Concentrating Solar Power (CSP) [3]–[5] belong to this type of systems.

In CSP systems used for production of electricity, a heat transfer medium is heated by the concentrated sunlight and then stored in insulated containers to produce electricity on demand, for example, utulizing a supercritical carbon dioxide (s-CO_2) Brayton power cycle, capable of yielding a thermal-to-electric conversion efficiency equal or greater than

WIT Transactions on Ecology and the Environment, Vol 261, © 2023 WIT Press
www.witpress.com, ISSN 1743-3541 (on-line)
doi:10.2495/ESUS230061

Figure 1: Heliostat field and central solar tower at Sandia NSTTF with solid particle reciever mounted on top of the tower.

50% [3]–[5]. The higher the temperature of the medium, the greater is the maximum achievable thermodynamic efficiency. Commonly used heat transfer media include molten nitrate salts, providing an operating temperature between 200 and 600°C [6], with problems due to corrosion and the need for high-quality airtight seals. An attractive alternative to salts as a medium is offered by inert particles, eliminating the corrosion effects and expanding the range of operating temperatures from subzero to >1000°C. Particles are exposed to concentrated sunlight while falling through an aperture (open on the side of the incoming solar radiation). Accordingly, systems of this type are referred to as FPR (falling particle receivers [7]). An important research FPR facility was developed at the Sandia National Laboratories (SNL) National Solar Thermal Testing Facility (NSTTF) (Fig. 1). The falling particle receiver forms part of the CSP Gen3 program issued by the US Department of Energy (DoE) and designed by SNL. It offers a favorable path to operating temperatures up to and above 700°C, with heat fluxes greater than 1 MW/m^2 by implementing the use of synthetic Silica-based bauxite particles of sub-millimeter size as heat transport and storage media.

As with molten salts, falling particles present their own challenges in CSP facility operation. One such challenge identified in the past decade is formation of plumes of particles expelled out of the receiver aperture during on-sun and off-sun operation which can lead to significant material and heat losses for the system [8] (Fig. 2). These particle plumes need to be characterized, and their negative effects possibly mitigated, for example, with changes in the aperture geometry. This motivation led to a collaboration between Sandia National Laboratories and University of New Mexico (UNM) in development and calibration of diagnostic techniques to characterize the escaping particle plumes during full-scale on-sun operation both in terms of heat and mass flow rates. To calibrate the diagnostics and assess their uncertainty, a laboratory facility (UNM Solar Simulator) was built where the relevant parameters (such as mass flow rate) could be both measured directly and from image-based diagnostics using both visible light and thermal imaging [8]–[12]. The current paper is a continuation of this work, with a focus on reliable quantification of the egress flow rate of particles being expelled out of the FPR cavity,which would also help calculate the advective losses of the system.

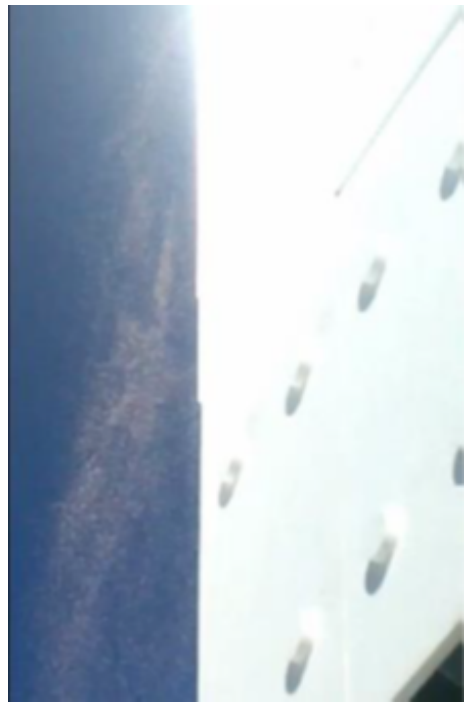

Figure 2: Particle egress captured from the falling particle receiver aperture during on-sun testing [8].

2 EXPERIMENTAL SETUP

In laboratory and in full-scale experiments, the same particles were used, CarboHSP [9] with a nominal mean diameter 330 μm and density 2 g/cm^3. The geometry of the imaging system was also kept consistent between laboratory and experiment, assuming a distance 5 m from the enclosure in full-scale tests.

2.1 Laboratory setup

The experimental setup at the University of New Mexico Solar Simulator was used for development and calibration of diagnostics. It consisted of the following components. At the top of the experimental rig (Fig. 3), an externally actuated furnace heated up the particles to the desired temperature for the experiment. A top hopper with an exchangeable bottom perforated plate for particle flow control was equipped with thermocouples to measure the temperature of the particles exiting the furnace. A sling gate started and stopped the particle flow. An interchangeable metallic mesh used to moderate the flow and provide a semi-uniform plume of falling particles. A bottom hopper collected the falling particles. It was equipped with thermocouples to measure the final temperature of the particles after falling. For infrared imaging, we employed a high-speed (300 frames per second) IR camera (ImageIR® 8300 hp) with a 100 mm lens at a resolution of 640×512 pixels situated 5 m from the particles curtain, as it would be the distance at which it would be located for full-scale on-sun tests at

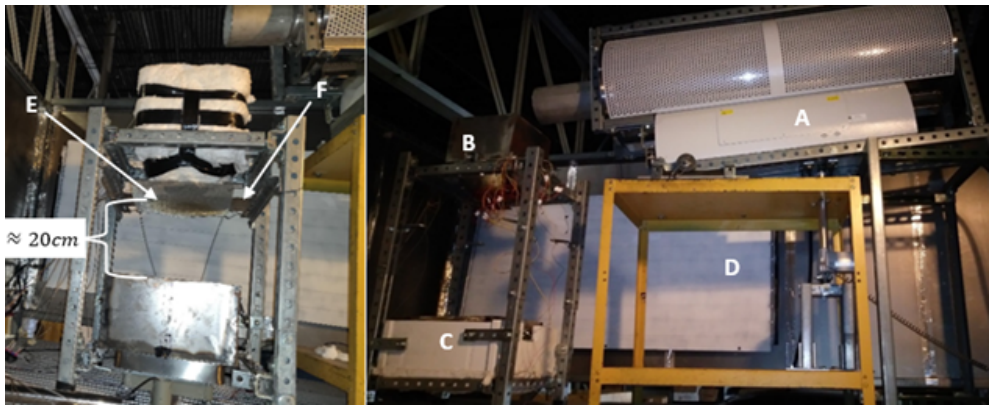

Figure 3: Experimental setup used at UNM Solar simulator facilities. The components are the following: (A) Furnace; (B) Top hopper; (C) Bottom hopper; (D) Cooled panel; (E) Metallic mesh; and (F) Sliding gate.

NSTTF. It should be noted that at this distance the pixel size is estimated to be 750 μm [9]. Mounted parallel with the IR camera was a visible-light camera (Nikon D3500 DSLR).

The main reason for using the high-speed IR camera was to extract the plume temperature as a function of time, however, if the spatial and temporal resolution were sufficient, it could also be used to estimate the bulk particle motion from the same sequences of thermograms that were used to quantify the temperature fields. Thus our goal was to make the IR camera will serve two purposes, 1) to measure the particle temperatures and 2) to measure the bulk particle velocity as a function of position for the calculation of the mass flow rate.

2.2 Full-scale setup

Once uncertainties in the diagnostics were quantified using the laboratory setup, we advanced to full-scale experiments at NSTTF. Like at the UNM Solar Simulator facilities, the cameras were situated 5 m apart from the point of interest, in this case, 5 m apart from the center of the aperture of the falling particle receiver. The IR camera along with the visible-light camera were placed inside a protective enclosure to prevent any damage for the particles being expelled out of the FPR aperture. The enclosure is equipped with a quartz window and an IR window to protect the camera lenses. The enclosure (Fig. 4) was then mounted on a testing stand positioning the cameras at the desired distance from the center of the FPR aperture.

3 EXPERIMENTS AND ANALYSIS

This section begins with the description of our laboratory results, which were mostly used to develop and validate the diagnostics, and follows with observations from NSTTF experiments.

3.1 Laboratory experiments for calibration of diagnostics

A set of tests were performed where about 5 kg of 330-micron CarboHSP 40–70 particles were pre-heated to six different temperatures (100, 200, 300, 450, 600, and 750°C) in the actuated furnace, then poured into the top hopper, where the heated particles where held until

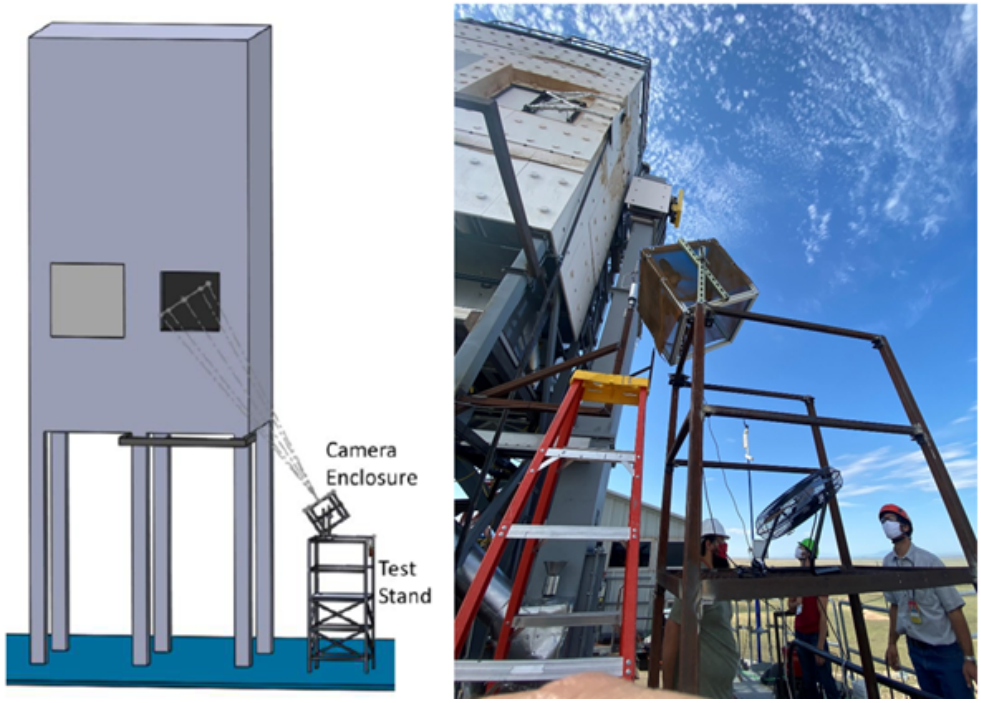

Figure 4: Left: CAD Design of camera test stand with enclosure next to the FPR. Right: photo of the camera enclosure and test stand prior to experiments.

all the equipment and members of the team were ready to proceed with the testing. Flow rates between 0.5 and 5 g/s were used in experiments, as confirmed by direct time-resolved measurements of mass of the particles collected. Once all the data acquisition systems were ready, the sliding gate was opened allowing for the particles to go through the restraining flow metallic mesh producing a curtain of falling particles. Once the curtain was formed, multiple sets of recordings were captured using the IR camera and the visible-light DSLR camera (Nikon D3500).

It was already known that in laboratory arrangements, steady-state particle curtains similar to ours develop velocity profiles very similar to free-fall, because the flow of the curtain is completely dominated by multiple gravity-driven particles, even at modest volume fractions comprising a dominant fraction of the mass in the curtain volume [13]. A parameter characterizing the respective role of particles and air in the flow is the multiphase Atwood number [14]

$$A_m = \frac{\rho_s - \rho_u}{\rho_s - \rho_u},$$

where in our case ρ_s is the volume-averaged density within the curtain (subscript s for "seeded"), and ρ_u is the unseeded air density. If $A_m \to 1$, the flow is dominated by the particle movement. A_m has its maximum value at the top of the particle curtain and decreases as the particles accelerate towards the bottom of the curtain. For a full characterization of the falling particle curtain flow, A_m is not enough, as it describes added mass due to the particle load, but does not describe how this mass is distributed: we can have the same multiphase

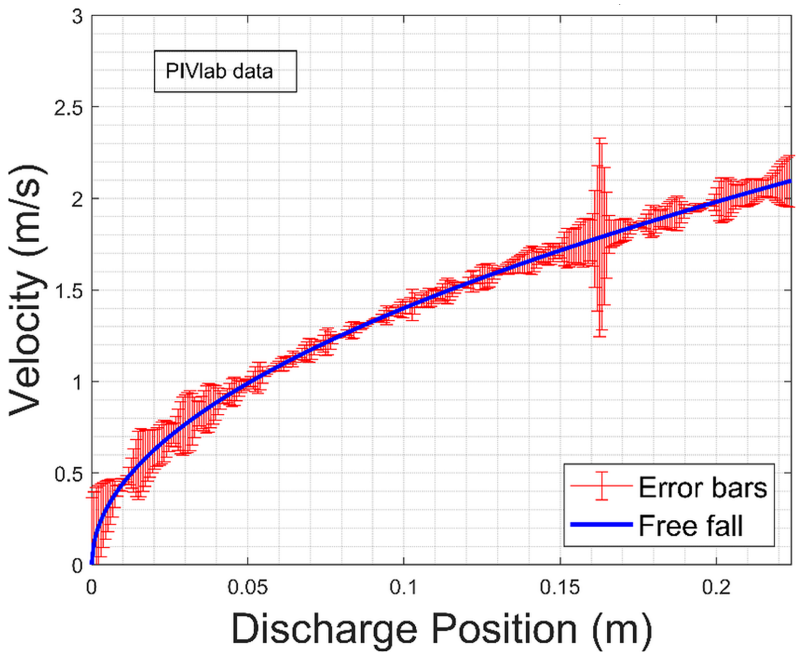

Figure 5: Uncertainty in velocity profile reconstruction (ensemble-average and 95% confidence intervals) at the center of the particle curtain (nominal width 10 cm, depth 1 cm) at 100°C. PIVlab was used for analysis. The flow rate is 5 g/s. "Free fall" curve represents theoretical velocity value with no drag.

Atwood number for a flow with many small particles or fewer large particles. In turn, the individual particle size influences the coupling between the particle and the surrounding air flow. For a single particle in a large volume of fluid, this coupling can be represented by the Stokes number $St = t_0 U l_0^{-1}$, where t_0 is the particle relaxation time, U is the characteristic flow velocity, and l_0 is the representative length scale. Particle behavior in falling particle curtains is further complicated by particles forming clusters and voids [13]. However, in the simple case of high A_m, submillimeter or micron-sized particles, and a modest size of the experimental apparatus, the average vertical velocity distribution of the particles is reliably parabolic.

This provided an opportunity for calibration of the two software suites we evaluated to extract velocity from the image sequences – open-source PIVlab [15] and proprietary DaVis [16]. Fig. 5 shows an example of uncertainty extracted from an ensemble of experimental datasets, with the deviation of the *average* velocity reconstruction from the free-fall result not exceeding 1 cm/s, and velocity vluctuations never exceeding 9 cm/s except in one place where the field of view in laboratory experiments had a low-contrast feature, leading to higher uncertainty (discharge position 0.16 m).

From the velocity measurements shown in Fig. 5 and the known mass flow rate, particle density, and air density (assuming the air temperature has equilibrated with the particles, near the top of the curtain (4 mm downstream position), $A_m = 0.91$. This value drops to 0.71 50 mm downstream and continues decreasing further, but overall, in the field of view we investigated at the flow rate 5 g/s, the assumption that the motion of the curtain is completely

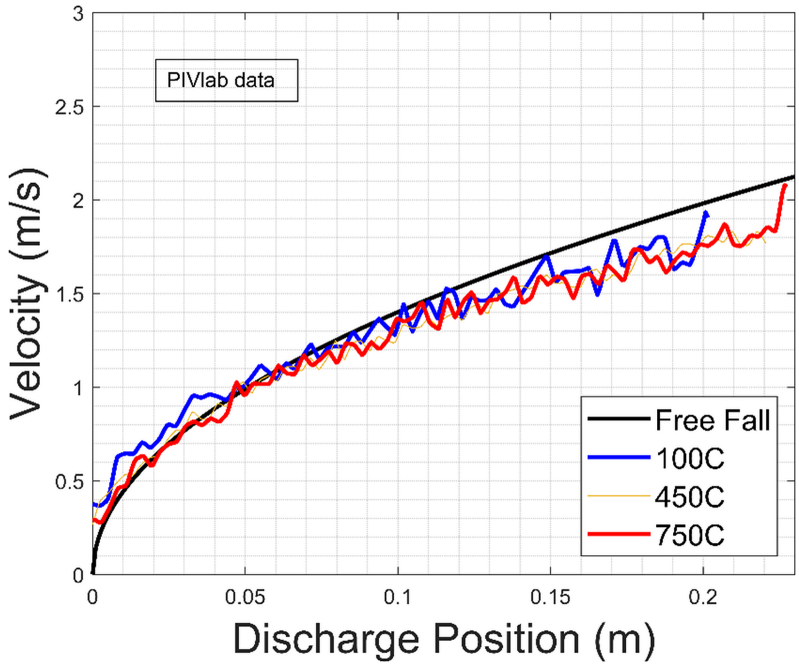

Figure 6: Comparison of instantaneous velocity profiles at three nominal particle temperatures (100, 450, 750°C) for the flow rate 0.5 g/s. PIVlab analysis data.

dominated by the particle inertia holds, and so we can calibrate the diagnostics using free-fall velocity. The flows we were able to produce in the lab span the range of multiphase Atwood numbers from where nearly-free-fall behavior should be expected ($A_m \to 1$) to lower values where velocity differences from free-fall emerge, and particle temperature begins to play a role due to changes in the viscosity of the air slowing particles down, as Fig. 6 shows. At 0.15 m position at particle temperature 450°C, the particle velocity is 1.58 m/s, appreciably slower than the free-fall value of 1.73 m/s, and the multiphase Atwood number for this flow rate and position is only 0.61, so viscous effects in air may begin to play a more noticeable role. It is also noteworthy that at low mass flow rates differences in particle velocities due to increase of air viscosity with temperature become noticeable.

The results above were produced with open-source PIVlab [15]. Commercial software DaVis [16] produced very similar velocity data, boosting our confidence in the validity of measurements (Fig. 7), but in the analysis of the on-sun experiments preference was used to PIVlab due to ease of integration within MATLAB.

3.2 On-sun experiments at NSTTF

Multiple tests were conducted at the Sandia NSTTF through which about 20 terabytes of data were acquired. For the tests conducted at the NSTTF, the data acquisition process differed from the process at the UNM lab facility by changes in the data sampling rate necessitated by the desire to capture intermittency absent from the lab experiments. While at the UNM solar simulator the IR camera was used to capture about 1 second of data with a sampling rate of 300 Hz, at the NSTTF the IR camera sampling rate was kept the same but it acquired

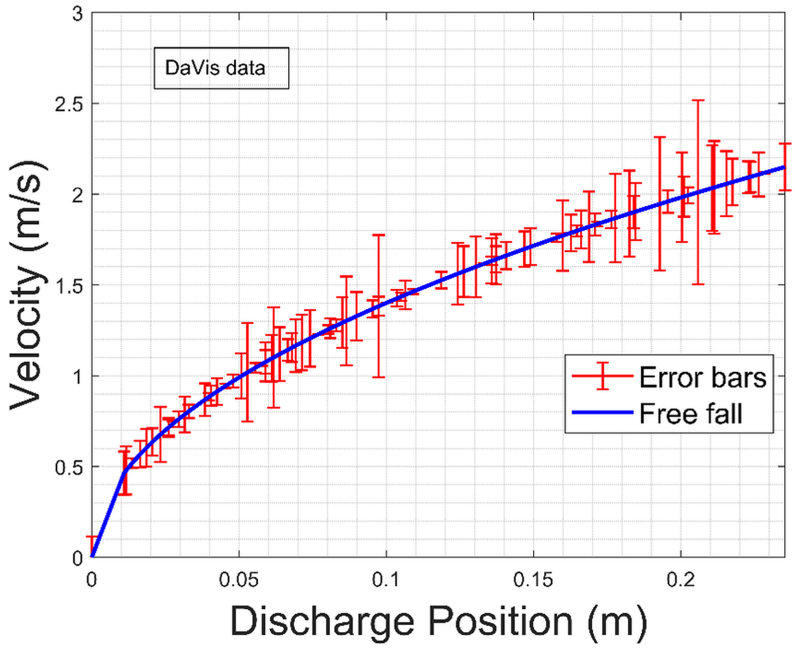

Figure 7: Velocity profile from the center of the particle curtain – average and fluctuations (95% confidence interval) and the expected free fall behavior at 100°C. DaVis analysis data.

2-minute time sequences every 2 minutes, resulting in a total of 36,000 thermograms per every 2 minutes of capturing data. Likewise, the sampling rate of the visual camera was kept close to that of the experiments conducted at the UNM facilities, but with a duration of 2 minutes. A detailed description of the tests is provided in our earlier papers [11], [12].

An initial attempt to extract plume velocities from raw thermogram data (Fig. 8) led to high fluctuations in the recovered velocity fields due to the PIV algorithm having difficulties in velocity extraction from images where both particles and a non-uniform intensity background was present. The same problem had been observed in the lab, as described in the previous subsection. An algorithm was developed to separate the particle images from the background in the thermograms [12], producing images of the particles agains a uniform background. Then, calculating the particle velocities and number counts, the particle egress rate from the FPR aperture could be quantified, and the FPR efficiency was estimated at 83%, which is an improvement in accuracy over the earlier estimates (79 to 83% [12]).

4 CONCLUSIONS

We developed a diagnostic technique to quantify efficiency losses in concentrating solar power receivers using falling particles as the thermal medium. The technique uses widely available particle-image velocimetry software, but applies to sequences of thermograms instead of visible-light images, which presents additional challenges (one of which was dealing with non-uniform image backgrounds). After laboratory calibration, we applied the analysis to a large set of thermogram data acquired at the Sandia National Laboratories NSTTF facility and achieved an improved estimate of the falling particle receiver efficiency.

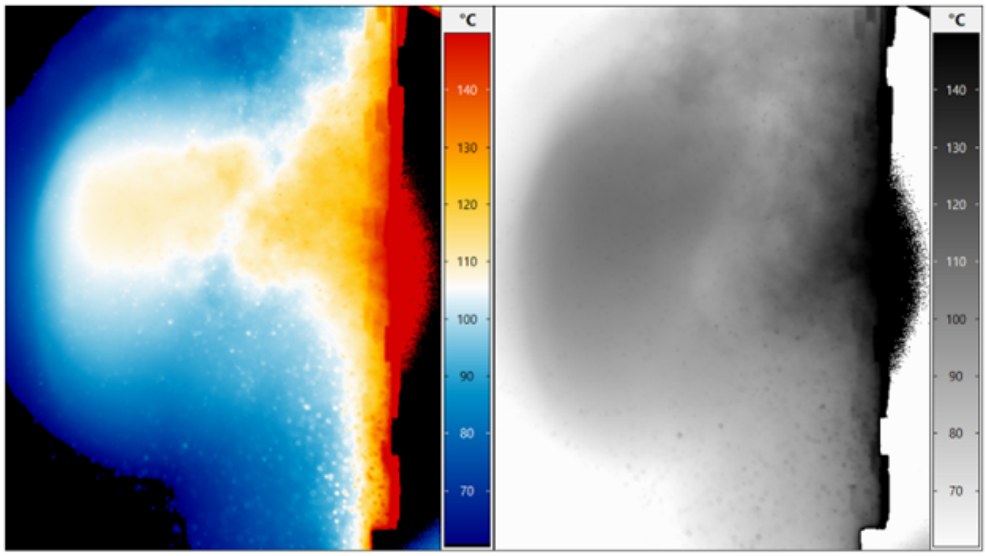

Figure 8: Example of an instantaneous thermogram of a plume escaping the FPR enclosure. Left – RGB palette, right – grayscale.

Based on the results of this work, for future studies it would be desirable to pair the high-speed IR camera with a high-speed visual-light camera, matching the framing rates to have a one-to-one comparison between the thermograms and the visual images. It would be beneficial if the latter also had a higher resolution than the thermograms. It would be worthwhile to deploy more cameras at different angles to better characterize the 3D properties of the particle plumes leaving the FPR cavity. These experiments would further improve the characterization of the advective losses of the system that can in turn lead to design improvements for the FPR.

ACKNOWLEDGEMENTS

This work was supported by Sandia National Laboratories via Standard Purchase Order 1915976. Professor Vorobieff also acknowleddges support from Halliburton Corporation.

REFERENCES

[1] Chandler, D.L., Shining brightly. *MIT News*, 26 Oct. 2011. https://news.mit.edu/2011/energy-scale-part3-1026. Accessed on: 30 Apr. 2023.
[2] Yang, L.H., Liang, J.D., Hsu, C.Y., Yang, T.H. & Chen, S.L., Enhanced efficiency of photovoltaic panels by integrating a spray cooling system with shallow geothermal energy heat exchanger. *Renewable Energy*, **134**, pp. 970–981, 2019.
[3] Ho, C.K., A review of high-temperature particle receivers for concentrating solar power. *Applied Thermal Engineering*, **109**, pp. 958–969, 2016.
[4] Ho, C.K., Advances in central receivers for concentrating solar applications. *Solar Energy*, **152**, pp. 38–56, 2017.
[5] Siegel, N.P., Ho, C.K., Khalsa, S.S. & Kolb, G.J., Development and evaluation of a prototype solid particle receiver: On-sun testing and model validation. *Journal of Solar Energy Engineering*, **132**(2), 2010.

[6] Fernández, Á.G. & Cabeza, L.F., Molten salt corrosion mechanisms of nitrate based thermal energy storage materials for concentrated solar power plants: A review. *Solar Energy Materials and Solar Cells*, **194**, pp. 160–165, 2019.
[7] Ho, C., Christian, J., Gill, D., Moya, A., Jeter, S., Abdel-Khalik, S., Sadowski, D., Siegel, N., Al-Ansary, H., Amsbeck, L. & Gobereit, B., Technology advancements for next generation falling particle receivers. *Energy Procedia*, **49**, pp. 398–407, 2014.
[8] Ho, C.K., Kinahan, S., Ortega, J.D., Vorobieff, P., Mammoli, A. & Martins, V., Characterization of particle and heat losses from falling particle receivers. *ASME 2019 13th International Conference on Energy Sustainability*, Washington, USA, 14–17 Jul. 2019.
[9] Ortega, J.D., Anaya, G., Vorobieff, P., Mohan, G. & Ho, C.K., Imaging particle temperatures and curtain opacities using an IR camera. *ASME 2020 14th International Conference on Energy Sustainability*, 17–18 Jun. 2020.
[10] Ortega, J.D., Vazquez, I.R., Vorobieff, P. & Ho, C.K., A simple and fast MATLAB-based particle size distribution analysis tool. *International Journal of Computational Methods and Experimental Measurements*, **9**(4), pp. 352–364, 2021.
[11] Ortega, J.D., Ho, C.K., Anaya, G., Vorobieff, P. & Mohan, G., A non-intrusive particle temperature extraction methodology using infrared and visible-image sequences for high-temperature particle plumes. *Journal of Solar Energy Engineering*, **145**(4), 041010, 2023.
[12] Ortega, J.D., Anaya, G., Ho, C.K., Vorobieff, P. & Mohan, G., Bulk velocity and mass flowrate estimation of particle plumes through particle image velocimetry analysis of thermogram sequences. *Journal of Solar Energy Engineering*, **145**(4), 2023.
[13] Ludwigsen, J., Wayne, P., Freelong, D., Vigil, G., Shaheen, C., Vorobeiff, P. & Truman, C.R., Fractal properties of a falling particle curtain in air. *Journal of Fluids Engineering*, **144**(1), 2022.
[14] Anderson, M., Vorobieff, P., Truman, C.R., Corbin, C., Kuehner, G., Wayne, P., Conroy, J., White, R. & Kumar, S., An experimental and numerical study of shock interaction with a gas column seeded with droplets. *Shock Waves*, **25**, pp. 107–125, 2015.
[15] Thielicke, W. & Stamhuis, E., PIVlab–towards user-friendly, affordable and accurate digital particle image velocimetry in MATLAB. *Journal of Open Research Software*, **2**(1), 2014.
[16] LaVision, Inc. DaVis – software solution for intelligent imaging. https://www.lavision.de/en/products/davis-software/. Accessed on: 30 Apr. 2023.